arXiv:hep-ph/0208140v1 14 Aug 2002

Interpreting data from WIMP direct detection experiments

Anne M Green
Physics Department, Stockholm University, Stockholm, 106 91, SWEDEN

Abstract. Weakly Interacting Massive Particle (WIMP) direct detection experiments are closing in on the region of parameter space where relic neutralinos may constitute the galactic halo dark matter. We discuss two issues in the interpretation of data, in particular the calculation of exclusion limits, from these experiments. Firstly we show that the technique that has been used for calculating exclusion limits from binned data without background subtraction produces erroneously tight limits, and discuss alternative methods which avoid this problem. We then argue that the standard maxwellian halo model is likely to be a poor approximation to the dark matter distribution and examine how halo models with triaxiality, velocity anisotropy and small scale clumping affect exclusion limits.

1. Introduction

Arguably the best motivated non-baryonic dark matter candidate is the neutralino (the lightest supersymmetric particle), and current direct detection experiments are just reaching the sensitivity required to probe the relevant region of parameter space [1]. The most stringent exclusion limits on Weakly Interacting Massive Particles (WIMPs) in general currently come from the Edelweiss [2] and Cryogenic Dark Matter Search (CDMS) experiments [3, 4], with competitive constraints also having been produced by experiments which have been optimized for double-beta decay such as Heidelberg-Moscow (HM) [5] and IGEX [6]. The exclusion limits from these experiments, calculated assuming a standard maxwellian halo, are plotted in Fig. 1 along with the region of parameter space corresponding to the DAMA collaboration's annual modulation signal [7]. Given the experimental progress, and the tension between the DAMA collaboration's annual modulation signal and the exclusion limits from other experiments, it is crucial to examine the assumptions involved in interpreting data from these experiments.

We focus on two separate issues: the calculation of exclusion limits with the correct coverage (i.e. which correspond to the stated degree of confidence) and the effect of halo modeling on exclusion limits. In Sec. 2 we show that the method previously used to calculate confidence limits from experiments without background subtraction and binned data (such as HM and IGEX) produces erroneously tight exclusion limits, and discuss alternative criteria for calculating exclusion limits. In Sec. 3 we turn our attention to the dependence of the theoretical differential event rate on the WIMP speed distribution. We discuss the properties of galactic halos and examine how models which reproduce these properties affect the exclusion limits from the HM and IGEX experiments.

2. Calculating exclusion limits

In experiments without background subtraction, such as Heidelberg-Moscow (HM) [5] and IGEX [6], any set of WIMP parameters (mass and cross-section) which would produce more events than are observed, at some confidence level, can be excluded at that confidence level.

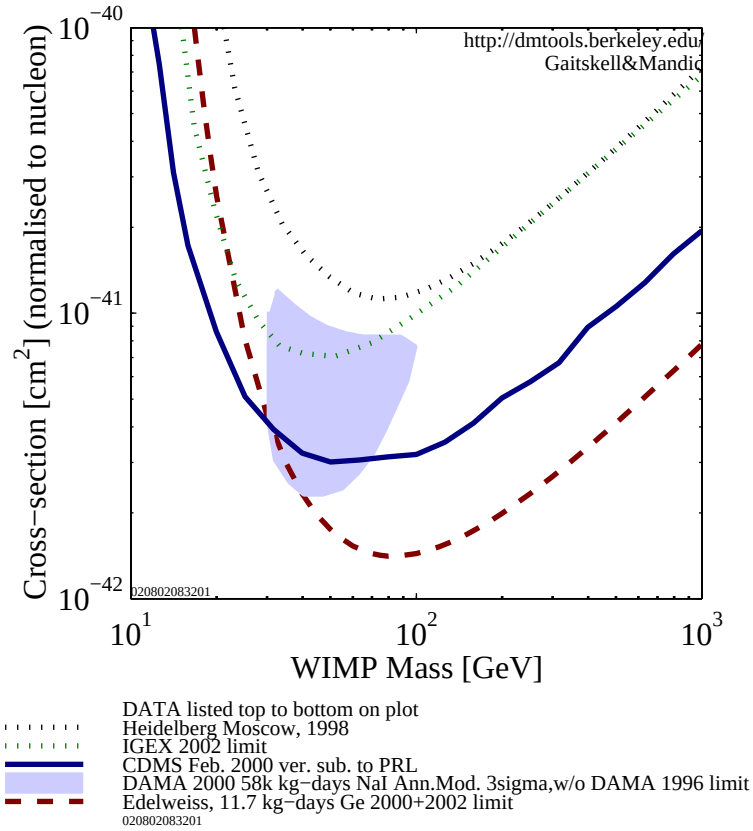

Figure 1. Exclusion limits, and the DAMA annual modulation region, from the WIMP direct detection experiments discussed in the text, assuming a standard maxwellian halo model, plotted using the interactive limit plotter at http://dmtools.berkeley.edu/limitplots/ .

The HM and IGEX collaborations have data in bins of width 1 keV (42 bins from 9 keV for HM and 45 bins from 4 keV for IGEX) and in their analysis [5, 6] the 90% confidence exclusion limit on the cross-section, $\sigma_{\rm p}$, is calculated by finding for each m_χ the value of $\sigma_{\rm p}$ for which the theoretical event rate in *one* of the bins just exceeds the 90% confidence limit on the event rate in that bin. By definition a 90% upper confidence limit means that there is a 10% probability that a theoretical number of events greater than the 90% confidence limit produced the observed number of events, *for any given bin*.

We will now consider an ensemble of bins, where $N_{\rm t}$ is the total number of bins, $N_{\rm e}$ is the number of bins for which the theoretical number of events exceeds the 90% bin confidence limit and $P(N_{\rm e})$ is the probability distribution of $N_{\rm e}$. For an ensemble of bins

$$\begin{aligned} P(N_{\rm e} > 0) &= 1 - P(N_{\rm e} = 0) = 1 - (0.9)^{N_{\rm t}} \\ &> 0.1 \quad \text{if } N_{\rm t} > 1\,. \end{aligned} \tag{1}$$

In other words the exclusion limits found using the standard analysis actually correspond to a lower degree of confidence than 90%, and are hence erroneously tight.

The probability distribution of the number of bins $N_{\rm e}$ exceeding their $100p\%$ (where $0 < p < 1$) bin confidence limit can be used to formulate criteria which produce true 90% minimum confidence exclusion limits (see Ref. [8] for further details). Firstly, for any given total number of bins, we can vary p and find the confidence level cl for which the probability that none of the bins exceed their $100cl\%$ bin confidence is 90%. For $N_{\rm t} = 45$, $cl = 0.9977$. We can also take $p = 0.9$ and calculate the 90% minimum upper confidence

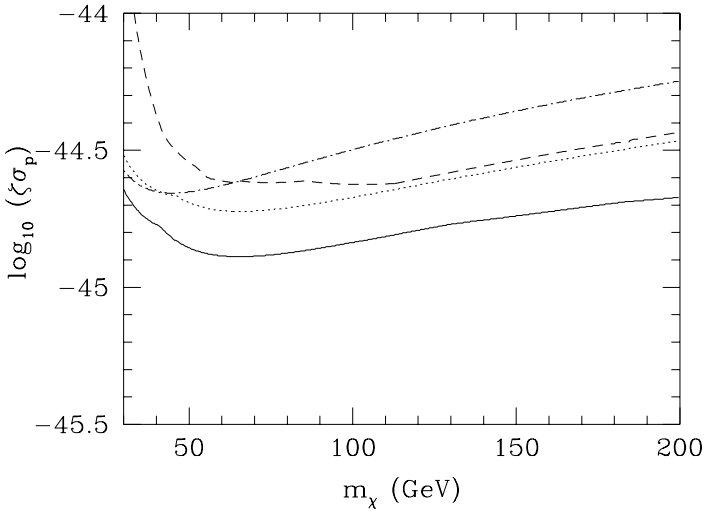

Figure 2. The spin-independent WIMP cross-section exclusion limits found from the IGEX 60 kg-day data [9], assuming the standard maxwellian halo model, from: using the standard no bin exceeding its 90% bin confidence limit method (solid), no bin exceeding its 99.77% bin confidence limit (dotted), no more than 7 bins exceeding their 90% bin confidence limit (dashed) and the lowest energy bin not exceeding its 90% bin confidence limit (dot-dashed).

limit on the number of bins which exceed their 90% bin confidence limit. For $N_{\rm t} = 45$, $P(N_{\rm e} < 8) = 0.924$. Since $N_{\rm e}$ can only take on integer values this criteria does not produce exact 90% exclusion limits, but the amount by which the confidence limits are stronger than 90% is known, and fixed for fixed $N_{\rm t}$. A simple minded way to avoid the problem of calculating correct overall confidence limits would be to discard all but one of the energy bins; $N_{\rm t} = 1$ then and the 90% bin confidence limit gives an overall 90% confidence limit. The obvious choice for the energy bin to use is the lowest, threshold, energy bin, since ${\rm d}R/{\rm d}E_{\rm R}$ decreases roughly exponentially with increasing $E_{\rm R}$ for the standard Maxwellian halo model so that this bin is often the most constraining. This wasteful method will of course produce weaker exclusion limits than can be found using the entire data set though.

The exclusion limits resulting from these criteria, assuming a standard maxwellian halo, are plotted in Fig. 2 for the IGEX 60 kg-day data [9]. We see that the standard technique produces exclusion limits that are erroneously tight (by roughly $\Delta(\log_{10}\sigma_{\rm p}) \sim 0.2.$ for $m_\chi > 80$ GeV). No more than 7 bins exceeding their 90% bin confidence limit produces exclusion limits which are especially weak for small m_χ and does not produce exactly 90% exclusion limits, since the number of bins is an integer. Only using one of the energy bins is wasteful and produces substantially weaker exclusion limits than could be found using the entire data set. Requiring that no bin exceeds its 99.75% bin confidence limit therefore appears to be the best of these methods for producing genuine 90% overall confidence limits.

Several other techniques have been proposed for dealing with this problem. The CRESST collaboration [10] carry out a maximum likelihood fit of their measured signal with an empirical function to effectively find the maximum WIMP signal which can be 'hidden' behind the background. Yellin [11] has devised an 'optimal interval method' for use with low background unbinned data, which has been used by the CDMS collaboration to calculate a limit from their data without Monte Carlo subtraction of the neutron background [4]. This method effectively chooses the binning of the data which gives the tightest exclusion limit, while taking into account the statistical 'penalty' associated with the freedom in the binning.

3. Milky Way halo modeling

The direct detection event rate and its energy distribution are determined in part by the WIMP speed distribution (see eq. 3 below). Data analyzes nearly always assume a standard smooth halo model with isotropic maxwellian velocity distribution. Belli et. al. [12] have recently reanalyzed the DAMA collaboration's annual modulation signal [7] for a range of halo models, finding that the allowed region of WIMP mass–cross-section parameter space is significantly enlarged. Models with triaxiality or velocity anisotropy may produce a significant change even in the mean differential event rate [13, 14]. Furthermore all of the non-standard halo models which have previously been considered are essentially smooth, while N-body simulations produce dark matter halos which contain significant amounts of substructure [15].

We first review the global and local properties of dark matter halos and then examine how these properties may affect the calculation of exclusion limits.

3.1. Review of halo properties

3.1.1. Global properties Observational constraints on the structure of dark matter halos depend on the relation of luminous tracer populations to the underlying density distribution, and are complicated by galactic structure and projection effects (see e.g. Ref. [16]). Given the difficulties involved in 'observing' dark matter halos it makes sense to turn to numerical simulations for information on their possible properties. In CDM cosmologies structure forms hierarchically, from the top down [17]. Small objects (often known as subhalos) form first, with larger objects being formed progressively via mergers and accretion. The internal structure of large galaxy size halos is determined by the dynamical processes which act on the accreted components, for instance the tidal field of the main halo can strip material away from a subhalo [18, 19] producing tidal streams along its orbit [20].

Current simulations of galaxy halos within a cosmological context can resolve sub-kpc scales (see e.g. [15, 21]). Discrepancies between the halos produced in these simulations (which have lots of surviving dwarf galaxy sized subhalos and steep central profiles) and observations, have led to claims of a crisis for the cold dark matter model (see Ref. [22] and references therein for an extensive discussion). Most relevant for the local dark matter distribution is the subhalo problem which may be, at least partly, due to complications in comparing the observed luminous matter with the dark matter distribution from the simulations. In particular it has been argued that gas accretion onto low mass halos may be inhibited after reionization so that a large fraction of the subhalos remain dark [23]. It has also been shown that if the observed dwarf galaxies themselves have dark halos, then their masses have been underestimated and correcting for this would go toward resolving the discrepancy with observations [19, 24]. The survival of subhalos is at least partly due to their concentrated profiles, so any modification to the simulations which produced halos with shallower central profiles could also reduce the number of surviving subhalos, however. Despite the ongoing debate regarding the detailed comparison of the small scale properties of simulated halos with observations, cosmological simulations may still provide us with useful information about the global properties of galactic halos.

The shape of simulated halos varies, not just between different halos of the same mass, but also as a function of radius within a single halo, strongly if the halo has undergone a major merger relatively recently. Two high resolution Local Group halos studied in detail in Ref. [25] have axis ratios of $1 : 0.78 : 0.48$ and $1 : 0.45.0.38$ at the solar radius and $1 : 0.64 : 0.40$ and $1 : 0.87 : 0.67$ at the virial radius. Adding dissipative gas to simulations tends to preserve the short-to-long axis ratio while increasing the intermediate-to-long axis

ratio [26].

The anisotropy parameter $\beta(r)$, defined as

$$\beta(r) = 1 - \frac{< v_\theta^2 > + < v_\phi^2 >}{2 < v_{\rm r}^2 >}\,, \tag{2}$$

where $< v_\theta^2 >$, $< v_\phi^2 >$ and $< v_{\rm r}^2 >$ are the means of the squares of the velocity components, also varies with radius. Typically $\beta(r)$ grows, although not monotonically, from roughly zero in the center of the halo to close to one at the virial radius, with non-negligible variation between halos (see Fig. 23 of Ref. [27]). The high resolution galactic mass halos studied in Ref. [28] have $\beta(R_\odot)$ in the the range 0.1-0.4, corresponding to radially biased orbits.

This broad picture, that galaxy halos are triaxial with anisotropic velocity distributions, is supported by various observations (see e.g. Refs. [16, 29, 30, 31]).

3.1.2. Local dark matter distribution The local dark matter distribution, which is crucial for direct detection experiments, can not be probed directly by cosmological simulations; the smallest subhalos resolvable in the highest resolution simulations have mass of order $10^7 M_\odot$ and it is not possible to fully resolve substructure within subhalos. Little substructure is found within the central regions of simulated halos, however it is not known whether the subhalos have been destroyed by tidal stripping or if this is purely a resolution effect [25]. This is relevant for the local dark matter distribution as the solar radius ($R_\odot \approx 8$ kpc) is small compared with the radius of the MW halo. The computing power required to directly probe the local dark matter distribution will probably not be available for a decade or so [25], therefore other numerical [25, 32] and semi-analytic [33] approaches have been used to address the problem. This work is reviewed in detail in Ref. [34]. In summary, there is currently no consensus on the local dark matter velocity distribution, with the results obtained depending on the method used to extrapolate to small scales below the resolution limit of the cosmological simulations. The local dark matter velocity distribution may be well approximated by a smooth multi-variate gaussian, with clumps of high velocity particles present if the MW halo has undergone a recent major merger [32], on the other hand it is possible that the local dark matter density could be zero or that a single dark matter stream with small velocity dispersion could dominate or that many tidal streams could overlap to give a smooth distribution [25].

3.2. Effect on exclusion limits

The differential WIMP event rate due to scalar interactions can be written in terms of the WIMP scattering cross section on the proton, $\sigma_{\rm p}$ [35]:

$$\frac{{\rm d}R}{{\rm d}E} = \zeta\sigma_{\rm p}\left[\frac{\rho_{0.3}}{\sqrt{\pi}v_0}\frac{(m_{\rm p}+m_\chi)^2}{m_{\rm p}^2 m_\chi^3}A^2 T(E)F^2(q)\right]\,, \tag{3}$$

where the local WIMP density, ρ_χ is normalized to a fiducial value $\rho_{0.3} = 0.3\,{\rm GeV/cm^3}$, such that $\zeta = \rho_\chi/\rho_{0.3}$, m_A is the atomic mass of the target nuclei, E is the recoil energy of the detector nucleus, and $T(E)$ is defined as [35]

$$T(E) = \frac{\sqrt{\pi}v_0}{2}\int_{v_{\rm min}}^{\infty}\frac{f_v}{v}{\rm d}v\,, \tag{4}$$

where f_v is the WIMP speed distribution in the rest frame of the detector, normalized to unity, and $v_{\rm min}$ is the minimum detectable WIMP speed

$$v_{\rm min} = \left(\frac{E(m_\chi+m_A)^2}{2m_\chi^2 m_A}\right)^{1/2}\,. \tag{5}$$

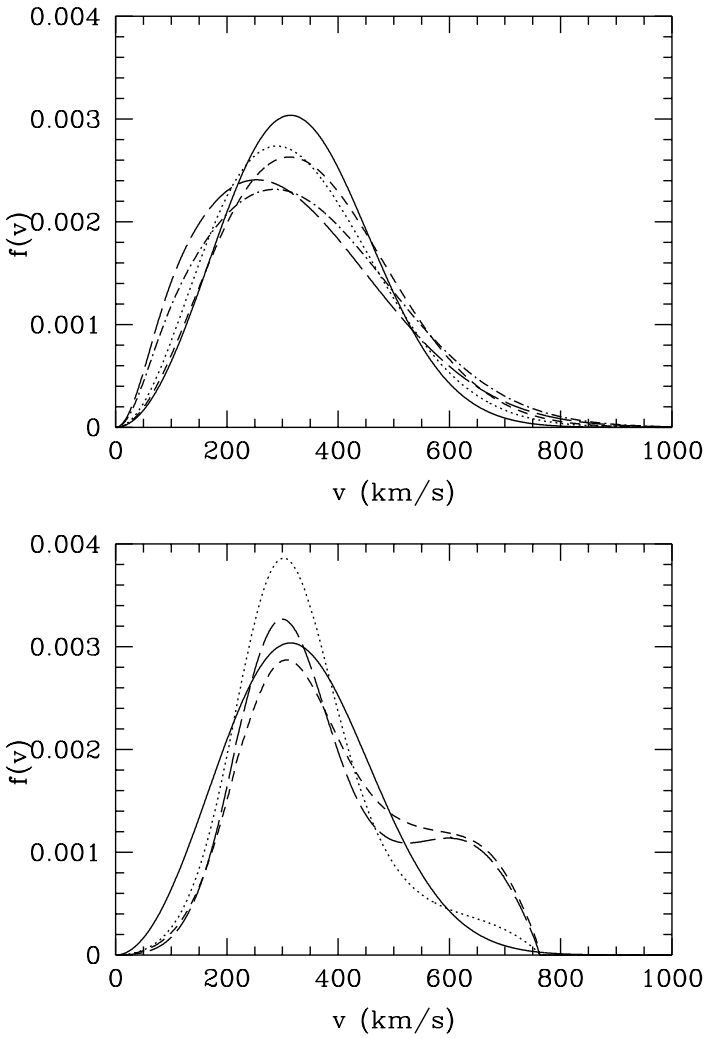

Figure 3. The speed distributions, in the rest frame of the Sun, for the standard halo model (solid line), and the logarithmic ellipsoidal model on the intermediate axis (upper panel) for p=0.9, q=0.8 and $\beta = 0.1/0.4$ (dotted/short dashed) and for p=0.72, q=0.7 and $\beta = 0.1/0.4$ (long dashed/dot dashed) and for the OM anisotropy model (lower panel) with $\beta = 0.13, 0.31$ and 0.4 (dotted, short-dashed, and long-dashed).

We will first examine the change in the WIMP speed distribution, and hence the exclusion limits, for triaxial and anisotropic, but still smooth, halo models. To date two self-consistent triaxial and/or anisotropic halo models have been studied in relation to WIMP direct detection: the logarithmic ellipsoidal model [13] and the Osipkov-Merritt anisotropy model [36], studied in Ref. [14]. We extend the previous work by focusing on parameters which span the range of observed and simulated halo properties.

The logarithmic ellipsoidal model [13] is the simplest triaxial generalization of the isothermal sphere and the velocity distribution can be approximated by a multi-variate gaussian on either the long or the intermediate axis ‡. We consider parameter values $p = 0.9, q = 0.8$ corresponding to axial ratios $1 : 0.78 : 0.48$ and $p = 0.72, q = 0.70$ corresponding to $1 : 0.45 : 0.38$, and values of the anisotropy parameter which give $\beta = 0.1$

‡ Of course there is no reason to expect the Sun to be located on one of the axes of the halo.

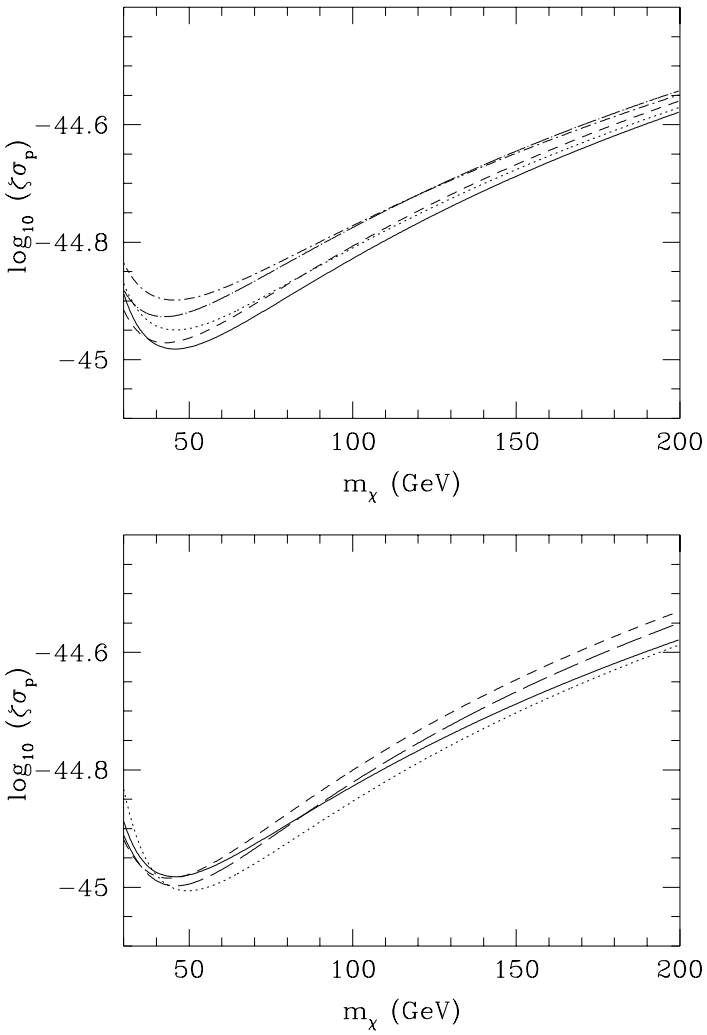

Figure 4. The exclusion limits from the IGEX experiment for the logarithmic ellipsoidal model, location on the intermediate axis (upper panel) and for the OM model (lower panel). Parameters and line types as in Fig. 3.

and 0.4. The speed distributions on the intermediate axis, in the rest frame of the Sun normalized to unity, are plotted in Fig. 3 along with that for the standard maxwellian halo model. For both positions the triaxial models have a wider spread in speeds than the standard model, so that the differential event rate will decrease less rapidly with increasing recoil energy, but the change is small on the major axis. This is because the change in the speed distribution is largely determined by the velocity dispersion in the ϕ direction. On the major axis, for parameter values which give $0.1 < \beta < 0.4$, all three components of the velocity have roughly the same dispersion, whereas on the intermediate axis the velocity dispersion in the ϕ direction is significantly larger than that in the z direction.

In the Osipkov-Merritt (OM) model, which assumes a spherically symmetric density profile, the velocity anisotropy varies as a function of radius as

$$\beta(r) = \frac{r^2}{r^2 + r_{\rm a}^2}\,, \tag{6}$$

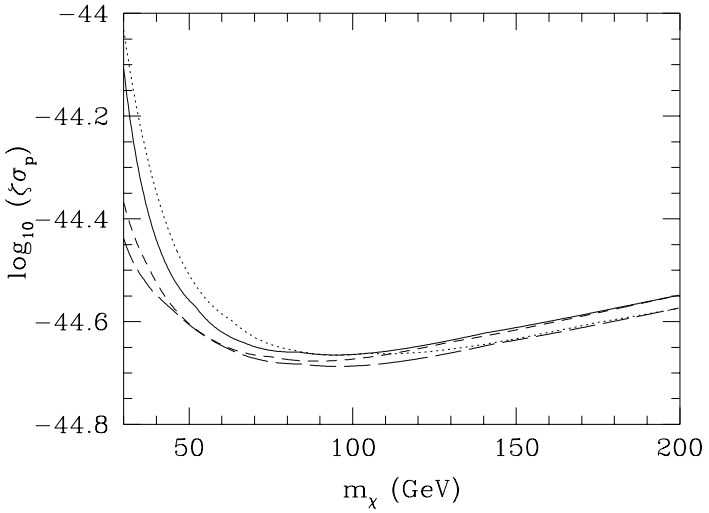

Figure 5. The exclusion limits from the HM experiment for the OM model. Parameters and line types as in the lower panel of Fig. 3.

so that the degree of anisotropy increases with increasing radius, as is found in numerical simulations. Following Ref. [14] we assume a NFW [37] density profile with scale radius $r_{\rm s} = 20$ kpc. We use values of the anisotropy radius $r_{\rm a} = 20, 12,$ and 9.8 kpc which correspond to $\beta(R_0) = 0.14, 0.31$ and 0.4 respectively. The resulting speed distributions are plotted in Fig. 3. The excess at large v is due to the increased number of particles on very elongated, nearly radial orbits [14].

To assess the effect of changes in the speed distribution on exclusion limits we need to take into account the detector response, including the difference between the observed energy of an event and the actual recoil energy, non-zero energy threshold and energy resolution (see Ref. [38] for further details), as these factors may blur out the effects of changes in the speed distribution. In Fig. 4 we plot the exclusion limits found from the IGEX data by requiring that the data in no more than one energy bin exceeds its 99.77% confidence limit, so as to produce 90% overall confidence limits (see above and Ref. [8]), for the logarithmic ellipsoidal model and for the OM anisotropy model. We also plot the exclusion limits from the Heidelberg-Moscow (HM) experiment [5] for the OM anisotropy model in Fig. 5. Comparing Figs. 4 and 5 we see that the change in the exclusion limits depends not only on the halo model under consideration, but also on the data being used; for IGEX the change in the exclusion limits is largest for large m_χ, while for HM the change is largest for small m_χ. For different m_χ, different energy ranges can be most constraining; for the IGEX data the lowest energy bin is always the most constraining, while for HM as m_χ increases the constraint comes from higher energy bins. It should therefore be borne in mind when comparing exclusion limits from different experiments, that changing the assumed WIMP speed distribution will affect the limits from different experiments differently.

The change in the exclusion limits is not huge (of order tens of per-cent) for the experiments we have considered, however these experiments are not optimized for WIMP detection. The change in the differential event rate, and hence the exclusion limit, would be significantly larger for an experiment with better energy resolution and lower threshold energy (see Ref. [34]). We have also seen that different models with the same value for the anisotropy parameter β have very different speed distributions, and hence a different effect on the exclusion limits . Furthermore it is conceivable that the local WIMP speed distribution

may deviate even further from the standard maxwellian distribution than the models that we have considered.

We will now turn our attention to the possibility that the local dark matter distribution is not smooth. Even if dynamical processes produce a smooth background dark matter distribution, late accreting clumps may lead to a local density enhancement and velocity clumping [33, 32], producing a shoulder in the differential event rate, if their density and velocity with respect to the earth are large enough [33]. For the experiments we have been considering the lower energy bins are most constraining, so that only very rare high density and velocity streams would have a non-negligible effect on the exclusion limits. The effect of these late accreting clumps on the annual modulation and directional signals would be more significant however [33].

Finally we look at the consequences of the more speculative possibility that small subhalos may survive at the solar radius. We could then be located within a subhalo with local density in excess of the mean value of $0.3\,\mathrm{GeVcm}^{-3}$, on the other hand it is even possible that we could be in a region between clumps and streams where the WIMP density is zero [25]. In the latter case all attempts at WIMP direct detection would be doomed to failure, and exclusion limits would tell us nothing about the WIMP cross-section. At the other extreme a tiny subhalo at the earth's location would produce a distinctive signal and, due to its high density, an enhanced event rate, making it easier to detect WIMPs of a given cross-section. Subhalos with $M \ll 10^9 M_\odot$ would have negligible velocity dispersion and hence a delta-function speed distribution [33]. The resulting theoretical differential event rate would be a step function with amplitude inversely proportional to the speed of the subhalo with respect to the earth, and position increasing with increasing relative speed and WIMP mass. Consequently for small subhalo velocities and WIMP masses there would be no constraint on the WIMP cross-section (no WIMPs would have sufficient energy to cause an observable recoil), but as the WIMP mass is increased the constraints would become much tighter as then all the WIMPs would be energetic enough to cause events of a given recoil energy.

In summary, triaxiality and velocity anisotropy lead to non-negligible changes in the exclusion limits, even for non-optimized detectors. Furthermore the changes are different for different data sets and depend on how the anisotropy is modeled. If the local WIMP distribution is dominated by small scale clumps then the density in the solar neighborhood may be zero (making it impossible to detect WIMPs) or significantly enhanced (making it easier to detect WIMPs with a given cross-section), and the exclusion limits are changed dramatically. Clearly the survival of subhalos at the solar radius is a very important issue for WIMP direct detection.

4. Conclusions

We have examined two aspects of the interpretation of data from WIMP direct detection experiments. We have seen that care needs to be taken when calculating exclusion limits from experiments without background subtraction so as to produce correct limits. Yellin's optimal interval method provides a sophisticated and robust solution to this problem for experiments with unbinned data and relatively small numbers of events [11], in other cases Poisson statistics can be used to formulate criteria which produce correct limits [8].

We have also seen that even if the local WIMP distribution is smooth its speed

distribution may deviate significantly from the standard maxwellian, and this has a non-negligible effect on exclusion limits and, crucially, effects the limits from different experiments differently. Constraints (and in the future possibly best fits) calculated assuming a standard maxwellian halo could be erroneous [14]. The derivation of reliable constraints on WIMP parameters and comparison of results for different experiments requires a theoretical framework for dealing with the uncertainty in the WIMP speed distribution. On the other hand, more optimistically, it might be possible to derive useful information about the local velocity distribution, and hence the formation of the galactic halo, if WIMPs were detected [33, 32].

References

[1] L. Bergström, Rept. Prog. Phys. **63**, 793 (2000).
[2] A. Benoit et. al., astro-ph/0206271.
[3] R. Abusaidi et. al., Phys. Rev. Lett. **84**, 5699 (2000).
[4] D. Abrams et. al., astro-ph/0203500.
[5] L. Baudis et. al., Phys. Rev D **59**, 022001 (1999).
[6] A. Morales et. al., Phys. Lett. B **532**, 8 (2002).
[7] R. Bernabei et. al., Phys. Lett. **B389**, 757 (1996); ibid **B408**, 439 (1997); ibid **B424**, 195 (1998); ibid **B450**, 448 (1999); ibid **B480**, 23 (2000).
[8] A. M. Green, Phys. Rev. D **65**, 023520, (2002).
[9] A. Morales et. al., Phys. Lett. B **489**, 268 (2000)
[10] M. Altmann et. al. paper contributed to 'The X International Symposium on Lepton and Photon Interactions at High Energies', July 2001, Rome, astro-ph/0106314.
[11] S. Yellin, physics/0203002.
[12] P. Belli, R. Cerulli, N. Forengo and S. Scopel, hep-ph/0203242.
[13] N. W. Evans, C. M. Carollo and P. T. de Zeeuw, Mon. Not. Roy. Astron. Soc. **318**, 1131 (2000).
[14] P. Ullio and M. Kamionkowski, JHEP 0103:049 (2001).
[15] A. Klypin, et. al. Astrophys. J, **522**, 82 (1999); B. Moore et. al., Mon. Not. Roy. Astron. Soc. **310** 1147 (1999).
[16] P. D. Sackett, Galaxy Dynamics, ASP Conf Series, 182, p393, eds. D. Merritt, J.A. Sellwood and M. Valluri, (1999).
[17] S. D. M. White and M. Rees, Mon. Not. Roy. Astron. Soc. **183**, 341 (1978); G. R. Blumenthal, S. M. Faber, J. R. Primack and M. J. Rees, Nature **311**, 517 (1984); M. Davis, G. Efstathiou, C. S. Frenk and S. D. M. White, Astrophys. J. **292**, 517 (1985).
[18] J. Binney and S. Tremaine, *Galactic Dynamics* (Princeton University Press, Princeton, NJ 1987).
[19] E. Hayashi, J. F. Navarro, J. E. Taylor, J. Stadel, & T. Quinn, astro-ph/0203004.
[20] A. Helmi and S. D. M. White, Mon. Not. Roy. Astron. Soc. **307**, 495 (1999).
[21] C. Power et. al., astro-ph/0201544.
[22] A. Tasitsiomi, astro-ph/0205464.
[23] J. S. Bullock, A. V. Kravtsov, and D. Weinberg, Astrophys. J, **539**, 517 (2000).
[24] F. Stoehr, S. D. M. White, G. Tormen, and V. Springel, astro-ph/0203342.
[25] B. Moore et. al., Phys. Rev. D **64**, 063508 (2001).
[26] N. Katz and J. E. Gunn, Astrophys. J. **377**, 365 (1991); J. Dubinski, Astrophys. J. **431**, 617 (1994).
[27] T. Fukushige and M. Junichiro, Astrophys. J., **557**, 533 (2001).
[28] B. Moore, T. Quinn, F. Governato, J. Stadel, and G. Lake, Mon. Not. Roy. Astron. Soc. **310**, 1147 (1999).
[29] R. P. Olling and M. R. Merrifield, Mon. Not. Roy. Astron. Soc. **311**, 361 (2000).
[30] R. Ibata, M. Irwin, G. F. Lewis and A. Stolte, Astrophys. J **547**, 133 (2001); R. Ibata, G. F. Lewis, M. Irwin, E. Totten and T. Quinn, Astrophys. J. **551**, 294 (2001).
[31] M. Odenkirchen, P. Brosche, M. Geffert and H. J. Tucholke, New. Astronomy **2**, 477 (1997).
[32] A. Helmi, S. D. M. White and V. Springel, astro-ph/0201289.
[33] D. Stiff, L. M. Widrow and J. Frieman, Phys. Rev. D **64**, 083516 (2001).
[34] A. M. Green, astro-ph/0207366.
[35] G. Jungman, M. Kamionkowski and K. Griest, Phys. Rep. **267**, 195 (1996).
[36] L. P. Osipkov, Pis'ma Astron. **55**, 77 (1979); D. Merritt, Astron. J. **90**, 1027, (1985).
[37] J. F. Navarro, C. S. Frenk, and S. D. M. White, Astrophys. J, **462**, 563 (1996); ibid **490**, 493 (1997).
[38] J. D. Lewin and P. F. Smith, Astropart. Phys. **6**, 87 (1996).